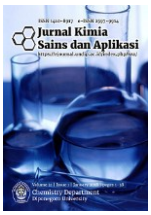
ISSN: 1410-8917
e-ISSN: 2597-9914

Jurnal Kimia Sains dan Aplikasi 29 (9) (2026): 618-630

Jurnal Kimia Sains dan Aplikasi
Journal of Scientific and Applied Chemistry

Journal homepage: http://ejournal.undip.ac.id/index.php/ksa



Adsorption of Pb(II) Ions from Artificial Liquid Waste by Vermicompost Humic Acid

Mayang Fauziah Putri Kuntjahjono [1], Rahmat Basuki [1,*], Elva Stiawan [1], Sultan Napoleon [1], Wikrama Sarweswara [1], Zidni Aghna Haqina [1], Robith Alzamzami [1], Nugroho Adi Sasongko [2], Nuha [2]

[1] Department of Chemistry, Republic of Indonesia Defense University, Bogor, 16810, Indonesia
[2] Research Center for Sustainable Production System and Life Cycle Assessment, National Research and Innovation Agency (BRIN), Banten 15314, Indonesia

* Corresponding author: rhmtbsq@gmail.com

https://doi.org/10.14710/jksa.29.9.618-630

Article Info

Article history:

Received: 11th June 2026
Revised: 13th September 2026
Accepted: 05th October 2026
Online: 30th October 2026

Keywords:
Vermicompost humic acid (VCHA); Pb(II) adsorption; heavy metal removal; wastewater treatment; sustainable adsorbent

Abstract

This study explores the use of vermicompost humic acid (VCHA) as a low-cost, eco-friendly adsorbent for the removal of Pb(II) from artificial liquid waste. VCHA was extracted and purified from vermicompost, then characterized using SEM-EDS, FTIR, and UV-Vis to determine its surface morphology, elemental composition, and functional groups. The characterization results confirmed the presence of oxygen-containing functional groups, such as carboxylate and phenolic hydroxyl groups, which are involved in metal binding. Adsorption studies demonstrated that the optimum pH for Pb(II) removal was 4, achieving a maximum removal efficiency of 96.78%. Equilibrium data were best fitted by the Langmuir isotherm model, yielding a maximum calculated adsorption capacity (q_{max}) of 129.05 mg/g. Kinetic data aligned most closely with the Ho pseudo-second-order model (k_{Ho} = 0.0012 g/mg), indicating that the rate of adsorption is governed by chemical interactions between Pb(II) ions and VCHA surface sites. These findings highlight the significant potential of VCHA as a waste-derived adsorbent for removing Pb(II) from an artificial liquid waste system.

1. Introduction

Water pollution from heavy metal waste is an increasingly serious environmental problem in Indonesia, driven by rapid industrialization, urbanization, and other anthropogenic activities. Heavy metals discharged into aquatic ecosystems are persistent, non-biodegradable, and bioaccumulative, posing severe long-term risks to surface water, groundwater, and public health [1]. Among heavy metals, lead (Pb) is one of the most dangerous pollutants because it is highly toxic even at low concentrations. Pb(II) ions are widely produced from industrial activities such as battery manufacturing, metal plating, paint and pigment production, mining, and the electronics industry. Accumulation of Pb(II) in the food chain causes severe physiological damage in humans, including neurological dysfunction, renal failure, and developmental disorders in children. Therefore, controlling and removing Pb(II) from liquid waste is a very important aspect of environmental protection and public health efforts [2].

Various technologies have been developed to treat liquid waste containing heavy metals, including chemical precipitation, ion exchange, membrane filtration, electrochemical processes, and adsorption. However, each method has limitations, such as the formation of hazardous sludge in chemical precipitation, high costs, and fouling in membrane technology, and operational complexity in electrochemical processes. Compared to other methods, adsorption is considered the most promising technique because it has high efficiency, a relatively simple process, lower operating costs, and flexibility in application and adsorbent regeneration [3]. The success of the adsorption process is greatly influenced by the characteristics of the adsorbent used, including surface area, pore structure, and the presence of active functional groups. Conventional adsorbents

such as activated carbon, zeolite, and synthetic resins have been widely used and show good adsorption capacity for Pb(II). However, the use of these adsorbents is often constrained by high production costs, complex synthesis processes, and the potential environmental impact of using hazardous chemicals. These conditions have encouraged the development of alternative adsorbents that are cheaper, environmentally friendly, and derived from renewable resources or organic waste.

Humic acid is the main fraction of humic compounds formed through the humification process of natural organic materials. This compound is known to have a high affinity for heavy metal ions because it contains various active functional groups, such as carboxylate (-COOH) and phenolic hydroxyl (-OH) groups. These groups enable interactions with metal ions through complexation, ion exchange, and electrostatic interactions. A number of studies have shown that humic acid is effective in adsorbing Pb(II) and other heavy metals from aqueous solutions [3]. However, most research and applications of humic acid as a heavy metal adsorbent still focus on humic acid derived from peat soil. The use of peat as a source of humic acid poses significant environmental problems, as peat extraction and drying can cause ecosystem degradation, reduce soil carbon reserves, and increase greenhouse gas emissions. Furthermore, peat-derived humic acids (PSHA) often exhibit lower functional group densities (typically total acidity around 5.0–6.5 meq/g) compared to biotransformed organic wastes. Therefore, alternative sources of humic acid that are more sustainable and do not cause significant negative environmental impacts are needed.

Vermicompost is the result of processing organic waste through the biological activity of earthworms, which produces material rich in humic and fulvic compounds. While raw vermicompost itself has been explored as a low-cost soil amendment, using raw waste directly as an adsorbent suffers from low adsorption capacity, organic leaching, and matrix interference. In contrast, purified VCHA (P-VCHA) isolated from raw vermicompost possesses significantly enhanced chemical properties. Biotransformation during vermicomposting accelerates the oxidation of organic matter, resulting in VCHA with higher total acidity (> 7.5 meq/g) and a higher concentration of carboxylate groups than traditional peat-derived HA. Utilizing vermicompost as a source of humic acid not only supports organic waste management but also aligns with the principles of circular economy and sustainable development [4].

Despite these advantages, previous studies have predominantly focused on raw vermicompost rather than the fundamental adsorption behavior of isolated, P-VCHA. A systematic knowledge gap remains regarding how the specific structural features, functional group density, and surface chemistry of P-VCHA quantitatively govern Pb(II) binding capacity and uptake rates from aqueous media. Therefore, this study aims to examine the ability of VCHA to adsorb Pb(II) from artificial liquid waste using UV-Vis analysis, determination of total acidity, carboxylate group content, and ash content, pH optimization, stability testing, and adsorption isotherm and kinetic modeling. The results of this study are expected to contribute scientifically to the development of environmentally friendly adsorbents based on humified organic materials for heavy metal waste treatment.

2. Experimental

2.1. Materials

The materials used in this study included humic acid from vermicompost from earthworms (*Eisenia fetida*) obtained from an earthworm farm in Lembang, West Java, 0.1 M NaOH solution, 36% HCl solution, $AgNO_3$ solution, HF, $Ba(OH)_2$, $Ca(CH_3COO)_2$, $PbCl_2$, and Alizarin Red S produced by Merck. Also used aluminum foil, universal indicator, Whatman 42 filter paper, and distilled water. All materials used had pro-analysis specifications.

2.2. Methods

2.2.1. Extraction of VCHA

Vermicompost was cleaned, dried, ground, and sieved through a 200-mesh sieve. A total of 500 g of dried vermicompost powder was dissolved in 5 L of 0.1 M NaOH under atmospheric conditions. The mixture was stirred for 24 h at room temperature and atmospheric pressure, then centrifuged at 3,000 rpm for 10 min to separate the filtrate from the residue. The filtrate was then filtered and slowly acidified with 0.1 M HCl to pH 1. The acidified filtrate was sealed and left to stand for 12–16 h until two layers formed. The upper layer contained fulvic acid, whereas the lower layer contained humic acid. The two layers were separated by centrifugation at 5,000 rpm for 15 min, and the resulting solid was collected as crude humic acid. The solid was then dried at 60°C for purification [5].

2.2.2. Purification of VCHA

A total of 50 g of crude humic acid was placed in a plastic container containing 250 mL of a 1:1 (v/v) mixture of 0.1 M HCl and 0.3 M HF to remove silica, clay, and other mineral impurities. The mixture was left to stand for 24 h at room temperature and atmospheric pressure. The mixture was then centrifuged at 5,000 rpm for 15 min to collect the solid. This purification process was repeated three times. The resulting solid was washed with distilled water to remove residual Cl^- ions from the extraction and purification processes. The presence of residual Cl^- ions was tested by adding $AgNO_3$ solution to the rinse water. Washing was continued until no white AgCl precipitate formed upon the addition of $AgNO_3$ solution. The chloride-free humic acid was then dried at 60°C and characterized using FTIR and UV–Vis spectroscopy [5].

2.2.3. Functional Group Test (Total Acidity and Carboxylate Content)

Total acidity was determined by indirect potentiometric titration using $Ba(OH)_2$ as the reagent. A 50 mg sample was placed in a 100 mL volumetric flask, and 20 mL of 0.1 M $Ba(OH)_2$ solution was added under a continuous nitrogen atmosphere. The flask was then

sealed and shaken for 24 h at room temperature and atmospheric pressure. A blank was prepared using the same procedure but without the sample. The resulting suspensions were filtered, and the residues were rinsed with CO_2-free distilled water. The filtrates and rinse waters were combined and titrated potentiometrically with standardized 0.5 M HCl until the pH reached 8.4. Each sample was analyzed in triplicate. Total acidity was calculated using Equation 1.

$$Total\ acidity\ (cmol/kg) = \frac{(V_b - V_s) \times N \times 10^5}{mg_{adsorbent}} \quad (1)$$

Where V_b is the volume of HCl used for the blank (mL), V_s is the volume of HCl used for the sample (mL), N is the normality of HCl (mol-equivalent/L), and $mg_{adsorbent}$ is the sample mass (mg).

Carboxylate content was determined using a similar indirect potentiometric titration method with $Ca(CH_3COO)_2$ as the reagent. A 50 mg sample was placed in a 100 mL volumetric flask, followed by the addition of 10 mL of 0.5 M $Ca(CH_3COO)_2$ solution and 40 mL of CO_2-free distilled water. A blank was prepared using 10 mL of 0.5 M $Ca(CH_3COO)_2$ solution and 40 mL of CO_2-free distilled water without the sample. The flasks were sealed and shaken for 24 h at room temperature and atmospheric pressure. The resulting suspensions were filtered, and the residues were rinsed with CO_2-free distilled water. The filtrates and rinse waters were combined and titrated potentiometrically with standardized 0.1 M NaOH until the pH reached 9.8. Each sample was analyzed in triplicate. Carboxylate content was calculated using Equation 2.

$$Carboxylate\ level\ (cmol/kg) = \frac{(V_s - V_b) \times N \times 10^5}{mg_{adsorbent}} \quad (2)$$

Where V_s is the volume of NaOH used for the sample (mL), V_b is the volume of NaOH used for the blank (mL), N is the normality of NaOH (mol-equivalent/L), and $mg_{adsorbent}$ is the sample mass (mg). The phenolic hydroxyl group content was calculated as the difference between total acidity and carboxylate content [5].

2.2.4. Ash Content Determination of VCHA

A 50 mg sample was placed in a porcelain crucible and heated in a furnace at 550°C for 4 h. The crucible and sample were weighed before and after heating. Each sample was analyzed in triplicate. The ash content was calculated using Equation 3.

$$Ash\ content\ (\%) = \frac{(M_3 - M_1)}{(M_2 - M_1)} \times 100\% \quad (3)$$

Where M_1 M_1 is the mass of the constant empty crucible (mg), M_2 is the mass of the crucible + sample before ignition (mg), M_3 mass of the crucible + ash after muffle furnace ignition (mg) [5].

2.2.5. Preparation of Alizarin Red S Complexing Solution

A 50 mg portion of Alizarin Red S was dissolved in distilled water in a 100 mL beaker. The solution was quantitatively transferred to a 100 mL volumetric flask, diluted to the mark with distilled water, and homogenized.

2.2.6. Stability Test of VCHA

Solutions at pH 4, 5, 6, 8, and 10 were prepared in separate flasks. Subsequently, 50 mg of P-VCHA was added to each solution. The mixtures were stirred for 120 min at room temperature and then left to stand for 24 h. The resulting solids were collected by filtration, dried, and weighed. VCHA stability was evaluated based on the mass of the residual solids, with a higher residual mass indicating greater stability under the tested conditions [6].

2.2.7. Determination of Optimum pH for Pb(II) Metal Adsorption

A 50 mg portion of P-VCHA was added to 30 mL of a 200 mg/L Pb(II) solution. The initial pH of the mixture was adjusted to the target values of 2, 4, 5, 6, and 8 using 0.1 M HCl or 0.1 M NaOH. The pH was measured with a calibrated pH meter before and after the adsorption process to monitor changes. The mixture was stirred for 120 min at room temperature and then filtered through Whatman No. 42 filter paper. The concentration of residual Pb(II) in the filtrate was determined using a UV–Vis spectrophotometer after complexation with Alizarin Red S. To correct for potential spectral interference from dissolved humic substances, a matrix blank consisting of VCHA filtrate without Pb(II), mixed with Alizarin Red S, was measured, and its absorbance was subtracted from that of the sample. The optimum adsorption pH was determined as the pH at which the highest amount of Pb(II) was adsorbed by VCHA [6].

2.2.8. Preparation of Standard Series Solution

A stock Pb(II) standard solution with a concentration of 200 mg/L, expressed as elemental Pb, was prepared by dissolving 0.2684 g of analytical-grade $PbCl_2$ in CO_2-free distilled water in a 1,000 mL volumetric flask. Working standard solutions with concentrations of 20, 30, 40, 50, and 75 mg/L were prepared by transferring 10, 15, 20, 25, and 37.5 mL of the stock solution, respectively, into separate 100 mL volumetric flasks and diluting each to the mark with distilled water. The absorbance of each standard solution was measured at the maximum absorption wavelength (λ_{max}) of 414 nm for the Pb(II)–Alizarin Red S complex using a UV–Vis spectrophotometer against an appropriate reagent blank.

2.2.9. Pb(II) Adsorption Isotherm Test Using VCHA

A 25 mg portion of P-VCHA was mixed with 30 mL of Pb(II) solutions at concentrations of 10, 20, 30, and 75 mg/L. The mixtures were stirred for 120 min at the optimum pH determined in the previous experiment. Each mixture was then filtered to collect the filtrate. The Pb(II) concentrations before and after adsorption were determined using a UV–Vis spectrophotometer after the addition of Alizarin Red S complexing solution.

2.2.10. Kinetic Adsorption Test of Pb(II) Using VCHA

A 25 mg portion of P-VCHA was mixed with 30 mL of a 50 mg/L Pb(II) solution at the optimum pH. The mixtures were stirred for 5, 10, 30, 50, 75, and 120 min to investigate the adsorption kinetics. These contact times were selected to capture both the rapid initial adsorption

phase and the subsequent approach to equilibrium. Preliminary results indicated that adsorption reached equilibrium within 50–75 min; therefore, a 120 min contact time was included to ensure sufficient time for equilibrium to be attained. After each contact time, the mixture was filtered, and the Pb(II) concentration in the filtrate was determined using a UV–Vis spectrophotometer after the addition of Alizarin Red S complexing solution.

3. Results and Discussion

3.1. Characterization of VCHA

The extraction process began with preparing vermicompost, which was then dried at room temperature to reduce its moisture content. The dried vermicompost was then sieved through a 100-mesh sieve to obtain finer particles, thereby increasing the surface area available for chemical interactions [7]. The resulting vermicompost powder was extracted using NaOH solution under alkaline conditions to dissolve the humic acid fraction from the complex organic matrix. Under these conditions, the carboxyl and phenolic hydroxyl groups in humic acid undergo deprotonation, increasing the solubility of humic substances [8]. The resulting filtrate, containing dissolved humic and fulvic acids, was then acidified with HCl to pH 1. At this low pH, humic acid precipitated as a dark brown solid, whereas fulvic acid generally remained soluble [9]. The protonation of acidic functional groups at low pH can reduce electrostatic repulsion between humic acid molecules and promote aggregation and precipitation [10].

Humic acid was purified through three treatment cycles using a mixture of HCl and HF to remove mineral impurities and other contaminants, thereby improving the purity of the extracted humic acid [11]. Residual chloride ions (Cl^-) from the HCl treatment were removed by repeatedly washing the purified humic acid with distilled water. The presence of residual Cl^- ions was tested by adding $AgNO_3$ solution to the washing filtrate. The absence of a white AgCl precipitate indicated that the chloride concentration was below the detection limit of this test. The reaction is shown in Equation (4) [8].

$$AgNO_3 + HCl \rightarrow AgCl\downarrow \text{ (white sediment)} + HNO_3 \quad (4)$$

The P-VCHA was then dried in an oven at 50°C for 24 h, ground, and sieved through a 200-mesh sieve to obtain fine particles with a more uniform size distribution. Smaller particle sizes can increase the specific surface area available for adsorption, potentially enhancing interactions between the adsorbent and heavy metal ions [12]. The resulting material was a fine, brown humic acid powder.

Scanning electron microscopy coupled with energy-dispersive X-ray spectroscopy (SEM–EDS) was used to characterize the surface morphology and elemental composition of VCHA. SEM provides information on surface topography and texture, whereas EDS identifies elements based on the characteristic X-rays emitted during electron-beam interactions with the sample [13]. As shown in Figure 1(a), the VCHA particles exhibited an irregular, rough, and heterogeneous surface morphology. Such features may be associated with the complex, heterogeneous structure of humic substances formed during the humification of organic matter. The observed surface heterogeneity may provide a variety of potential adsorption sites for Pb(II) ions. However, surface morphology alone cannot confirm the presence, number, or binding strength of these sites.

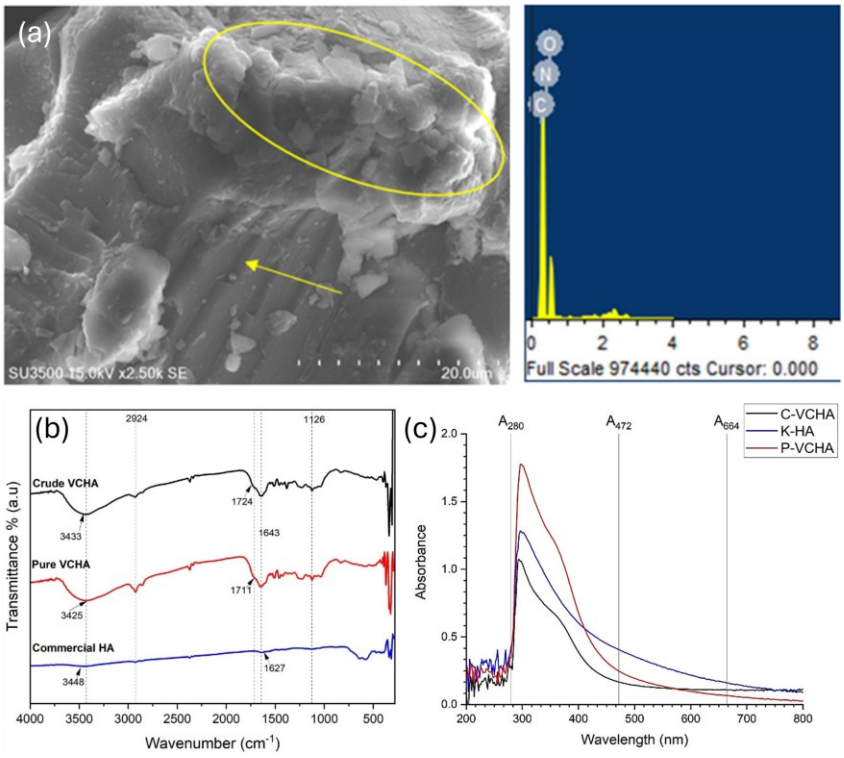


Figure 1. (a) SEM–EDS image of Pure VCHA (P-VCHA), (b) FTIR Spectrum of crude VCHA (C-VCHA), P-VCHA, and commercial HA (K-HA), and (c) Characteristic UV-Vis spectrum of C-VCHA, C-VCHA, and K-HA

Table 1. Absorbance ratio of extracted humic acid and commercial humic acid

Type of humic acid	A_{280}	A_{472}	A_{664}	E_2/E_6	E_2/E_4	E_4/E_6
P-VCHA	0.34588	0.24672	0.06632	5.21531	1.40191	3.72014
C-VCHA	0.28381	0.16679	0.10760	2.63763	1.70160	1.55009
K-HA	0.42793	0.40585	0.15980	2.67790	1.05440	2.53973

The VCHA particles exhibited an aggregated morphology, with irregular shapes and rough surfaces lacking distinct crystalline boundaries, suggesting a predominantly amorphous structure. At a magnification of 2,500× (Figure 1(a)), layered features, microcracks, and cavities were observed. These features may have developed during the extraction and purification processes and may provide pathways for Pb(II) ions to access potential adsorption sites. Fine cracks and aggregates of smaller particles were also visible on the VCHA surface.

The elemental composition of VCHA was analyzed using EDS, as shown in Figure 1(a). The results indicated that carbon (C) and oxygen (O) were the predominant elements, accounting for 61.26% and 38.05%, respectively, while nitrogen (N) accounted for 0.69%. This composition is consistent with the organic nature of humic substances, which contain carbon-based structures and various oxygen-containing functional groups. The oxygen content may be associated with functional groups such as carboxyl and phenolic hydroxyl groups, which are potential interaction sites for Pb(II) adsorption.

FTIR spectroscopy was used to identify the functional groups present in VCHA. The spectrum exhibited characteristic absorption bands associated with hydroxyl, aliphatic C–H, carbonyl, aromatic, and C–O-containing groups. These spectral features indicate the presence of various oxygen-containing functional groups in VCHA. However, FTIR results alone cannot establish whether a specific functional group directly binds Pb(II). Therefore, these groups are considered potential interaction sites rather than experimentally confirmed binding sites.

Based on Figure 1(b), the FTIR spectra of P-VCHA, C- VCHA, and K-HA exhibit relatively similar absorption band patterns, with no significant differences in wavenumbers. All three samples show a broad band in the range of 3425–3448 cm^{-1}, which is associated with the stretching vibrations of hydroxyl (–OH) groups. The presence of this band is a dominant characteristic of humic compounds due to the high content of oxygen-containing functional groups. The O–H band in the range of 3400–3450 cm^{-1} in humic acid has also been reported by Basuki *et al.* [6] in humic acid derived from horse manure. Furthermore, the band at 2924 cm^{-1} is attributed to aliphatic C–H stretching vibrations, indicating the presence of aliphatic hydrocarbon chains in the structure of humic acid [6].

A weak absorption band in the region of 1711–1724 cm^{-1} indicates the C=O stretching vibration of carboxylic (–COOH) groups and represents residual open-chain ketone or aldehyde structures [5]. Furthermore, a sharp absorption band in the range of 1627–1643 cm^{-1} suggests the presence of aromatic C=C vibrations and C=O stretching from quinone groups conjugated within an aromatic system. This band may also be associated with aromatic rings stabilized by hydrogen bonding of –OH groups [6]. The absorption band around 1126 cm^{-1} is attributed to C–O stretching vibrations of carboxylate groups. This band serves as an indicator of the presence of ether and alcohol functional groups within the humic acid structure [6]. The similarity in band positions and patterns among the three samples indicates that they share the same fundamental chemical framework as humic acid, with only minor differences due to variations in purity levels and impurity content. Therefore, the extraction and purification processes do not alter the fundamental structure of humic acid; rather, they enhance its purity without eliminating its characteristic functional groups.

The success of humic acid extraction from VCHA can be identified through a characteristic absorption pattern in the UV-Vis spectrum, namely the appearance of a strong peak in the 250–300 nm wavelength range and a smooth downward curve without any specific peaks up to around 800 nm (Figure 1(c)) [14]. This absorption pattern reflects the general characteristics of humic acid compounds, where high absorption intensity in the UV region is due to $\pi \rightarrow \pi^*$ electronic transitions from conjugated aromatic systems and organic chromophores, while the gradual decrease in absorbance reflects increasing aromatic structural complexity and degree of humification.

There are three important absorption regions that provide insight into the molecular composition of VCHA. Absorption at a wavelength of around 280 nm is related to the transformation of lignin and quinone components into humic structures. The 460–480 nm region indicates the presence of organic material in the early stages of humification, while absorption at 600–670 nm indicates the presence of highly humified material with a high content of aromatic groups. The degree of humification and level of aromatic complexity of VCHA can be analyzed through absorbance ratios such as E2/E6 (A280/A664), E2/E4 (A280/A472), and E4/E6 (A472/A664). The E2/E4 ratio value describes the comparison between the initial lignocellulose component and more mature humic material, while the E2/E6 ratio shows the proportion between the unhumified and fully humified organic fractions. Meanwhile, the E4/E6 ratio reflects the level of aromatic condensation and the degree of maturity of humic material. The lower the E2/E4, E2/E6, and E4/E6 ratios, the higher the level of humification and the greater the content of condensed aromatic structures in VCHA [15].

The results of UV-Vis spectrophotometer analysis in Figure 1(c) show that all humic acid samples display the characteristic absorption pattern of humic acid with a strong peak in the 250–300 nm region and a smooth decrease in absorbance up to 800 nm. Based on the absorbance data in Table 1, P-VCHA exhibits the highest absorption intensity at 280 nm, exceeding those of C-VCHA and K-HA. Although P-VCHA shows the highest absolute A280 value, the ratio between wavelengths shows a significant difference in the level of humification.

The E_2/E_6 ratio (A_{280}/A_{664}) of P-VCHA was higher than those of K-HA and C-VCHA, indicating that P-VCHA still contained a proportion of organic material that had not been fully humified. However, this was accompanied by a relatively high E_4/E_6 ratio compared with those of K-HA and C-VCHA, suggesting that the purification process increased the relative proportion of conjugated aromatic compounds. The higher E_4/E_6 ratio at this stage does not directly indicate complete humification but may reflect the removal of some non-aromatic fractions during purification, making the remaining aromatic fractions relatively more dominant, although their size and degree of condensation remain moderate. Meanwhile, the E_2/E_4 ratio of 1.40191 for P-VCHA supports the interpretation that lignin and humic precursors have undergone transformation toward more complex aromatic structures, but have not yet formed large, highly condensed aromatic structures or reached the degree of humification observed in commercial humic acid, which has a lower E_2/E_4 ratio of 1.054.

In addition, compared with C-VCHA, P-VCHA exhibited changes in its UV–Vis absorption spectrum following purification, including increased absorbance in the UV region (280 nm) and a relative decrease in absorbance in the visible region (472–664 nm). These changes may indicate differences in the relative contributions of aromatic chromophores and other organic fractions. This observation is consistent with the findings of Rani *et al.* [11], which reported that humic acid purification increased the relative contribution of aromatic chromophores and enhanced absorption in the 250–300 nm region through the removal of aliphatic compounds and polysaccharides. Therefore, P-VCHA exhibited a more pronounced spectral profile, potentially reflecting changes in the composition of its humic components, although its humification level may still differ from that of commercial humic acid.

3.2. Total Acidity, Carboxylate Group Content, and Ash Content of VCHA

The total acidity, carboxyl group (–COOH) content, and phenolic hydroxyl group (–OH) content of humic acid extracted from vermicompost were quantitatively determined using established analytical methods. Total acidity was determined based on the reaction between acidic functional groups in humic acid and $Ba(OH)_2$. In this process, protons (H^+) released from the acidic groups react with hydroxide ions (OH^-) to form water, while Ba^{2+} ions interact with the deprotonated functional groups to form barium salts. Humic acid can be represented as RH, where R denotes the humic macromolecular structure, and H represents an acidic proton. Upon reaction with excess $Ba(OH)_2$, the acidic groups release protons, and the remaining unreacted $Ba(OH)_2$ is subsequently titrated potentiometrically with HCl to determine the amount of residual base. The difference between the amounts of $Ba(OH)_2$ initially added and remaining after the reaction is used to calculate the total acidity of the humic acid [8]. The reactions are represented by Equations (5) and (6).

$$2RH + Ba(OH)_2 \text{ (excessive)} \rightarrow R_2Ba + 2H_2O \quad (5)$$

$$Ba(OH)_2 \text{ (remaining)} + 2HCl \rightarrow BaCl_2 + 2H_2O \quad (6)$$

The carboxyl group (–COOH) content was determined using calcium acetate [$Ca(CH_3COO)_2$], based on the reaction between the carboxyl groups of humic acid (R–COOH) and calcium acetate (Equation (7)). The release of H^+ ions from the carboxyl groups leads to the formation of acetic acid, while Ca^{2+} ions interact with the deprotonated carboxyl groups. The amount of H^+ released is proportional to the carboxyl group content. The acetic acid formed is subsequently titrated potentiometrically with NaOH (Equation (8)) to determine the carboxyl group content.

$$2R\text{-}COOH + Ca(CH_3COO)_2 \rightarrow Ca(R\text{-}COO)_2 + 2CH_3COOH \quad (7)$$

$$CH_3COOH + NaOH \rightarrow CH_3COONa + H_2O \quad (8)$$

The phenolic hydroxyl (–OH) content was determined indirectly by subtracting the carboxyl group content from the total acidity. This assumes that total acidity accounts for both carboxyl and phenolic hydroxyl groups, whereas the calcium acetate method primarily measures carboxyl groups.

The results of the functional group analysis of vermicompost humic acid are presented in Table 2. The total acidity of VCHA was substantially higher than that reported for humic acids from several other sources. This difference suggests that VCHA contains a relatively high concentration of acidic functional groups, including carboxyl and phenolic hydroxyl groups, which may be associated with the oxidation and humification of organic matter [16]. The high total acidity may be related to the characteristics of vermicompost, in which organic matter undergoes microbial and enzymatic degradation mediated by earthworms (*Eisenia fetida*) and associated microorganisms. These processes may contribute to the formation of oxygen-containing functional groups in humic substances [16, 17].

However, VCHA had a relatively lower carboxyl group content and higher phenolic hydroxyl content than some other humic acids. This difference may reflect variations in organic matter composition and transformation during humification. The degradation of lignin and polyphenolic compounds may contribute to the formation of phenolic structures, while organic matter oxidation may introduce carboxyl groups [18]. The relative abundance of these functional groups depends on factors such as the source material, microbial community, and humification conditions. Therefore, further comparative studies under standardized conditions are needed to evaluate differences in functional group composition among humic acids from different sources.

Table 2. Functional group contents of humic acids

Material	Total acidity (cmol/kg)	-COOH (cmol/kg)	Phenolic -OH (cmol/kg)
Vermicompost humic acid (extracted in this study)			
P-VCHA	1840	198	1642
Comparative humic acid			
C-HDHA [15]	493	316	177
C-PSHA [14]	690	432	258
HDHA [14]	513	330	183
PSHA [14]	753	472	281
CDHA [8]	500	250	250
PSHA (Schnitzer, in Stevenson)	560–890	150–570	20–490

Table 3. Ash content of VCHA and commercial compost

Material	Ash content (%)
P-VCHA	2.58
C-VCHA	12.94
K-HA	38.9

The difference between the results of this study and those reported in the literature may be due to differences in the methods and characteristics of the samples used. Factors such as base concentration, solid-to-solution ratio, extraction time, acidification process, and purification stage greatly affect the amount of acid groups measured. In addition, the possibility of residual salts or inorganic ions that have not been completely removed can also cause the total acidity value to appear higher, because the $Ba(OH)_2$ titration method is sensitive to all acid protons, both organic and inorganic [11].

This comparison shows that VCHA has unique chemical characteristics, with the highest total acidity and dominance of phenolic –OH groups. Functionally, the dominance of phenolic –OH groups in VCHA strengthens its complexation capacity toward metal cations through electron pair donation and π-metal interactions, while carboxylate groups provide ion exchange sites and the formation of stable bidentate complexes [16, 19]. The combination of the two gives VCHA high adsorption potential and multipoint binding, despite its relative composition differing from that of other humic acids.

Furthermore, the results of ash content analysis in this study are shown in Table 3, which indicates that the ash content in P-VCHA is much lower than that in dirty C- VCHA (before purification) and K-HA. The measured ash reflects the non-volatile inorganic mineral content remaining after the thermal combustion process. This ash mainly consists of metal oxides such as Fe_2O_3, Al_2O_3, CaO, and SiO_2, which are incorporated during the vermicomposting process. Low ash content indicates that the organic fraction is dominant and that humification has occurred optimally, thereby supporting thermal stability and implying good adsorption efficiency, as few active sites are covered by inert minerals. Meanwhile, a high ash content may indicate the presence of inorganic residues that have not been completely eliminated during the extraction and purification process [5, 20].

3.3. Stability Test and Optimum pH for Pb(II) Metal Adsorption

The stability of organic adsorbents, such as humic acid, refers to their ability to retain their structural integrity and solid content under varying environmental conditions, including changes in pH [21]. This property is important because the dissolution or dispersion of humic substances may affect the availability of functional groups, such as –COOH and –OH, for heavy metal adsorption.

The stability of VCHA was evaluated in distilled water at pH 4, 5, 6, 8, and 10 to investigate its behavior under different pH conditions, particularly in relation to the protonation and deprotonation of its functional groups. As shown in Figure 2(a), VCHA exhibited relatively high stability under acidic conditions (pH 4–5), as indicated by its resistance to dissolution under these conditions. This behavior may be attributed to the protonation of acidic functional groups, particularly –COOH, which reduces electrostatic repulsion between humic molecules and promotes aggregation. Intermolecular interactions, including hydrogen bonding, may also contribute to the stability of the resulting aggregates [5, 22].

However, VCHA stability decreased as the pH increased toward neutral and alkaline conditions. At pH 6, 8, and 10, the residual mass decreased markedly, indicating increased dissolution and the formation of negatively charged humate species through the deprotonation of acidic functional groups [21]. Under alkaline conditions, deprotonation of –COOH groups to $-COO^-$ groups and, at sufficiently high pH, some phenolic –OH groups to $-O^-$ groups increases the negative charge of humic substances. The resulting electrostatic repulsion can promote particle dispersion and dissolution in water. Changes in ionization may also affect hydrogen-bonding interactions that contribute to the association of humic molecules [23].

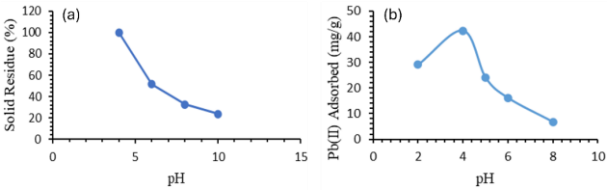


Figure 2. (a) VCHA stability test results curve, (b) Optimum pH curve for Pb(II) adsorption on VCHA

The results suggest that VCHA retains more of its solid phase under acidic conditions, particularly at pH 4–5, whereas the decrease in residual mass at pH 6 indicates the onset of increased dissolution. Retention of the solid phase may be beneficial for heavy metal adsorption because it can reduce adsorbent loss into the aqueous medium. However, residual mass alone does not establish that the molecular structure remains intact or that all active functional groups remain available. Under alkaline conditions, deprotonation may increase the negative charge of humic substances and favor interactions with metal cations, but increased dissolution may affect adsorbent recovery and reuse. Therefore, pH should be controlled to balance VCHA dissolution and adsorption performance.

The optimum pH for Pb(II) adsorption by VCHA was investigated by varying the solution pH to 2, 4, 5, 6, and 8. This analysis aimed to evaluate the effect of pH on the interaction between Pb(II) ions and the VCHA surface. The concentrations of Pb(II) before and after adsorption were determined using UV–Vis spectrophotometry. A decrease in absorbance indicated a reduction in the concentration of Pb(II) remaining in the solution and was used to assess adsorption efficiency. This decrease was consistent with the removal of Pb(II) from the solution during adsorption onto VCHA [24].

In this study, Pb(II) solutions at pH 2, 4, 5, 6, and 8 were contacted with VCHA for 120 min. The residual Pb(II) concentrations were determined by measuring the absorbance at the maximum wavelength of 414 nm, yielding values of 0.386, 0.356, 0.397, 0.415, and 0.436, respectively. As shown in Figure 2(b), the highest Pb(II) adsorption occurred at pH 4, where the lowest absorbance indicated the lowest residual Pb(II) concentration. The calculated adsorption capacity (q_e) was 42.4 mg/g, identifying pH 4 as the optimum pH under the tested conditions. This result is consistent with previous studies reporting that Pb(II) adsorption by humic acid often reaches its optimum at approximately pH 4–6. Within this range, carboxyl groups begin to deprotonate, increasing the negative charge of the adsorbent and promoting the binding of metal cations through ion exchange and complexation [14, 25, 26].

Solution pH influences the protonation state of the adsorbent's functional groups and the potential formation of metal-containing precipitates. At lower pH values, the functional groups of VCHA are more protonated, and competition between H^+ and Pb^{2+} for binding sites may reduce adsorption [6]. At pH 4, partial deprotonation of carboxyl groups increases the availability of negatively charged sites that can bind Pb^{2+} [25]. However, at higher pH values, the increase in absorbance suggests that the residual Pb(II) concentration increased and the apparent adsorption efficiency decreased. This trend may reflect changes in the surface chemistry of VCHA and the aqueous speciation of Pb(II). The formation of lead hydroxide or other lead-containing species may also affect the measured concentration at higher pH values; therefore, precipitation should be considered when interpreting the adsorption results [6].

3.4. Metal Complexation

Pb was selected as the target metal ion to evaluate the adsorption performance of VCHA. Before analysis, Pb(II) ions were complexed with Alizarin Red S, a chelating agent capable of forming complexes with metal ions. In this complex, Pb(II) acts as the central metal ion, while Alizarin Red S serves as the ligand. The ligand coordinates with the metal ion through its donor atoms, forming a metal–ligand complex [27].

Alizarin Red S contains a quinone-based structure with hydroxyl groups that can participate in complex formation. Pb^{2+} ions interact with the donor groups of Alizarin Red S, forming coordinate bonds [27]. This complexation alters the electronic structure of the ligand and produces a change in the solution's color. The resulting Pb–Alizarin Red S complex exhibits a yellow color under the conditions used in this study [28]. The proposed formation of the Pb–Alizarin Red S complex is illustrated in Figure 3(a).

The analysis of VCHA performance in absorbing Pb(II) ions began with measuring the maximum wavelength of Pb(II), which was found to be 414 nm. The absorbance data obtained were used for further analysis of Pb(II) metal. The data plot of concentration (X) versus absorbance (Y) for standard Pb(II) at concentrations of 0, 20, 30, 40, 50, and 75 mg/L yielded the equation y = 0.0027x + 0.2489 with a correlation coefficient of 0.999. A correlation coefficient value close to 1 indicates that the regression results are linear, as shown in Figure 3(b). This regression equation is then used as a quantitative reference to determine the concentration of Pb(II) ions in the sample after adsorption by VCHA.

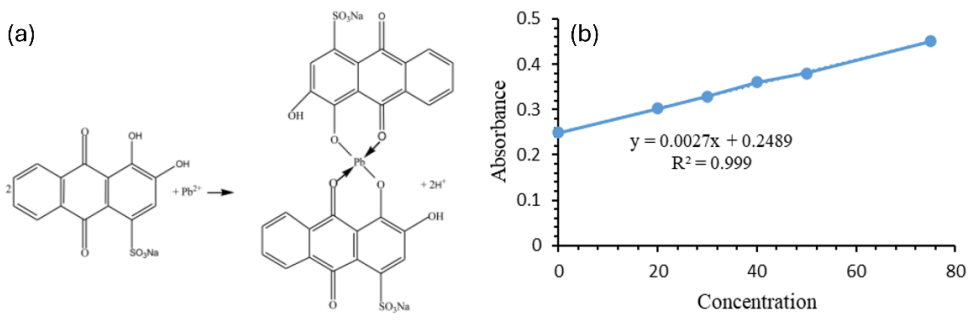


Figure 3. (a) Pb-Alizarin Red S metal complexation reaction and (b) Standard solution curve of Pb (II) metal

3.5. Adsorption Isotherms of Pb(II) on VCHA

Adsorption isotherms describe the relationship between the amount of adsorbate retained by an adsorbent and the equilibrium concentration of the adsorbate in solution [29]. In this study, Pb(II) adsorption by VCHA was investigated using initial Pb(II) concentrations of 10, 20, 30, and 75 mg/L. Isotherm modeling was used to characterize the adsorption behavior and evaluate the affinity of VCHA for Pb(II) ions.

Based on the coefficients of determination (R^2) presented in Figure 4, the Langmuir model provided the best fit to the experimental data, with an R^2 value of 0.9970. Although this high value indicates a strong empirical fit to the Langmuir equation, it does not definitively establish surface homogeneity or monolayer adsorption at the molecular level. According to the Langmuir parameters listed in Table 4, the calculated maximum adsorption capacity (q_{max}) and adsorption energy parameter (E_L) were 129.0463 mg/g and 23.9490 kJ/mol, respectively.

However, the calculated q_{max} value of 129.0463 mg/g must be interpreted with caution as a model-dependent theoretical estimate, given that the highest initial concentration evaluated in this study was 75 mg/L. Nevertheless, this high theoretical capacity reflects the strong binding potential of VCHA, which can be attributed to its high total acidity and dense availability of $-COO^-$ and phenolic $-OH$ groups that facilitate coordination with Pb(II) ions [30]. The E_l value of 23.9490 kJ/mol falls within the range typical for ion-exchange or weak chemical interactions (8–40 kJ/mol), suggesting that electrostatic attraction and ion exchange play a major role in the binding process [14]. Furthermore, the dimensionless separation factor (R_L) values ranged from 0.1490 to 0.5677 ($0 < R_L < 1$), confirming that the adsorption of Pb(II) onto VCHA is thermodynamically favorable under the experimental conditions evaluated.

Pb(II) adsorption onto VCHA was also evaluated using the Freundlich isotherm model to analyze parameters associated with multilayer adsorption. Based on Table 4, this model also shows a good fit, as indicated by an R^2 value of 0.9914. The Freundlich model assumes a heterogeneous adsorbent surface with non-uniform adsorption energy across all active sites. The Freundlich adsorption capacity (B) of 10.2343 mg/g and the n value of 1.3941 indicate that the adsorption system is favorable, as $n > 1$.

The Dubinin–Radushkevich (D–R) isotherm model was applied to provide complementary insights into the adsorption mechanism and to estimate the mean free energy of adsorption (E_{DR}) on energetically heterogeneous surfaces [6]. As shown in Table 4, the D–R model yielded a high determination coefficient (R^2 = 0.9967). However, it should be clarified that the D–R model describes adsorption onto Gaussian-distributed heterogeneous microporous structures rather than providing evidence for multilayer adsorption. The calculated D–R adsorption capacity (q_{DR}) of 1473.2001 mg/g represents a mathematical fitting parameter from the empirical equation rather than a physical indication of multilayer formation or pore-filling capacity. The primary significance of the D–R model lies in the mean adsorption energy (E_{DR}), which was calculated to be 9.5759 kJ/mol. An E_{DR} value within the range of 8–16 kJ/mol indicates that the adsorption process is predominantly driven by an ion-exchange mechanism or weak chemical interactions, rather than physical physisorption (E < 8 kJ/mol). This finding is highly consistent with the energy parameters derived from the Langmuir model (E_l), confirming that ion exchange between Pb(II) ions and the active carboxyl and phenolic hydroxyl groups of VCHA plays a central role in the binding process.

Table 4. Isotherm parameters for Pb(II) adsorption onto VCHA

Isotherm model	Parameter	Value
Langmuir	q_{max} (mg/g)	129
	K_L (L/mol)	1.58×10^4
	E_L (kJ/mol)	23.9
	R^2	0.997
Freundlich	K_F	10.2
	n	1.39
	E	-
	R^2	0.991
Dubinin–Radushkevich (D–R)	q_m (mg/g)	1.47×10^3
	β ($\times 10^{-9}$ mol^2/J^2)	5.45
	E (kJ/mol)	9.58
	R^2	0.997
Temkin	B (J/mol)	105
	K_T (L/g)	1.10
	R^2	0.964

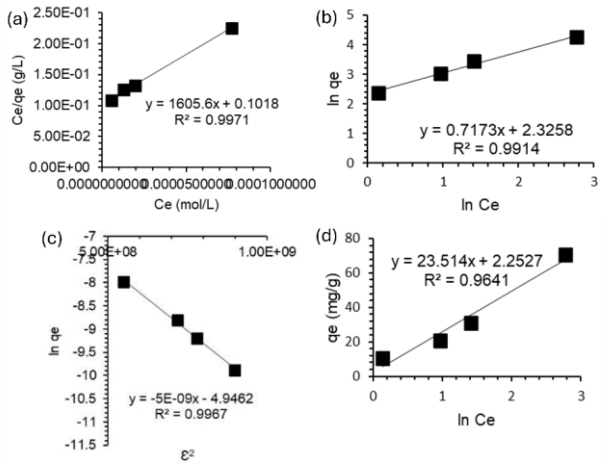


Figure 4. Linearized plots of the adsorption isotherm models: (a) Langmuir, (b) Freundlich, (c) Dubinin–Radushkevich (D–R), and (d) Temkin for Pb(II) adsorption onto VCHA

Table 5. Comparison of Langmuir adsorption capacity (b) for Pb(II) adsorption by various types of humic acid adsorbents at 298 K

Pb(II) Adsorbent	b (mg/g)	Optimum pH	Reference
Peat humic acid (Poland)	82.3	5	[31]
Peat humic acid–starch	58.0	6	[30]
MHDHA	57.6	5.5	[14]
Ground humic acid (India)	19.2	6	[32]
Ground humic acid (Riau)	23.12	5	[25]
VCHA	129	4	This study
Peat humic acid	15.0	5.5	[33]

The Temkin isotherm model considers the effects of adsorbate–adsorbent interactions on the adsorption process. It assumes that the heat of adsorption decreases linearly with increasing surface coverage [14]. As shown in Table 4, the Temkin constant related to the heat of adsorption (B) was 105.36 J/mol. The Temkin model yielded an R^2 of 0.964, which was lower than that of the Langmuir model (R^2 = 0.997). This result indicates that the Langmuir model provided a better fit to the experimental data than the Temkin model. However, the Temkin model may still describe the adsorption behavior associated with changes in adsorption energy as surface coverage increases.

3.6. Kinetic Adsorption of Pb(II) on VCHA

Adsorption kinetics analysis describes the rate and mechanism of adsorption, including the interaction process between metal ions as adsorbates and the surface of the adsorbent [34]. In this study, the adsorption rate of Pb(II) ions onto VCHA was analyzed to determine the effectiveness of the contact time required for the adsorbent to remove metal ions from the solution.

In this study, the adsorption rate of Pb(II) onto VCHA was analyzed over a contact time range of 5–120 minutes. The amount of Pb(II) adsorbed at equilibrium (Exp. q_e) was 18.4260 × 10^{-5} mol/g, under the following experimental conditions: V = 30 mL, T = 298 K, m = 0.0250 g, C_o = 50 mg/L, and pH = 4. To identify the adsorption mechanism, a comparative analysis of the models was conducted as shown in Figure 5(a–e). The Lagergren kinetic model (pseudo-first-order) indicates that rapid physical adsorption predominates in the initial stage of the process. In contrast, the Ho kinetic model (pseudo-second-order) suggests that chemisorption is the primary mechanism controlling the adsorption rate over longer periods [35]. Based on the data in Table 6, the Lagergren model shows a reasonably good R^2 of 0.9645; however, its calculated adsorption capacity (Calc. q_e) of 3.4921 × 10^{-5} mol/g does not closely match the experimental value. This indicates that although rapid physical adsorption occurs at the initial stage, it is not the rate-determining step of the overall process.

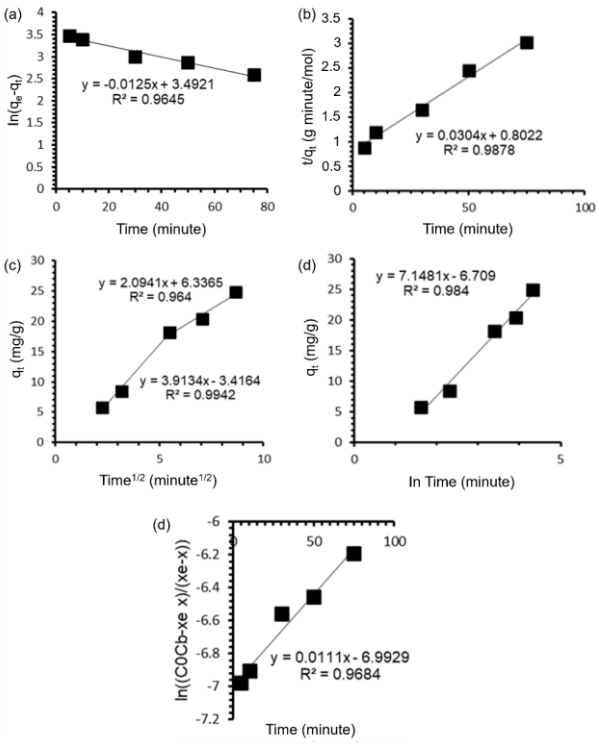


Figure 5. Adsorption of Pb(II) onto VCHA based on kinetic models: (a) Lagergren, (b) Ho, (c) Weber–Morris intraparticle diffusion, (d) Elovich, and (e) RBS kinetic model

Table 6. Kinetic parameters for Pb(II) adsorption onto VCHA

Kinetic model	Parameter	Value
Lagergren	Calc. q_e (× 10^{-5} mol/g)	3.49
	k_1 (min^{-1})	0.0125
	R_1^2	0.9645
Ho	Calc. q_e (× 10^{-5} mol/g)	32.9
	k_2 (g/mol min)	0.0012
	R_1^2	0.9878
Weber–Morris intraparticle diffusion	$k_{IPD,1}$ (mg/g $min^{1/2}$)	3.91
	$k_{IPD,2}$ (mg/g $min^{1/2}$)	2.09
	C_1 (mg/g)	-3.42
	C_2 (mg/g)	6.34
	$R_{IPD,1}^2$	0.9942
	$R_{IPD,2}^2$	0.9639
Elovich	α (mg/g min)	2.80
	β (g/mg)	0.140
	R^2	0.9839
RBS	Calc. q_e (× 10^{-5} mol/g)	16.4
	k_1 ($(mol/L)^{-1}$ min^{-1})	14.1
	k_2 (min^{-1})	0.0029
	K (L/mol)	4.79 × 10^3
	E (kJ/mol)	21.0
	R_1^2	0.9683

Table 7. Comparison of parameters obtained from kinetic and isotherm models for Pb(II) adsorption onto VCHA

Parameter	Experimental	Lagergren model	Ho model	RBS model	Langmuir model
Exp. q_e ($\times 10^{-5}$ mol/g)	18.43	3.49	32.9	16.4	-
K (L/mol)	-	-	-	4.79×10^3	1.58×10^4
E (kJ/mol)	-	-	-	20.99	23.95

In contrast, the Ho model exhibits an R^2 value closer to unity (0.9878) and a Calc. q_e of 32.8709×10^{-5} mol/g, which is closer to the experimental value. This suggests that Pb(II) adsorption is better described by the Ho kinetic model, indicating that the process is dominated by chemisorption, specifically ionic (electrostatic) interactions between the negatively charged adsorbent surface and positively charged metal cations [6]. The Elovich model also supports the dominance of chemisorption, with an R^2 value of 0.9839. Furthermore, the α and β parameters in the Elovich model represent the initial adsorption rate and the desorption rate, respectively. The higher value of α compared to β indicates that Pb(II) interacts effectively with VCHA and that the desorption rate is relatively low.

The Weber–Morris intraparticle diffusion model for Pb(II) adsorption onto VCHA exhibits a two-stage pattern, as indicated by the presence of two linear regions (IP-1 and IP-2). The first stage (IP-1) represents film diffusion or external mass transfer, namely the movement of Pb(II) ions from the solution to the outer surface of the adsorbent [6]. This is supported by the higher rate constant value of $k_{(IP-1)}$ (3.9133 mg/g.min$^{1/2}$) compared to $k_{(IP-2)}$ (2.0940 mg/g.min$^{1/2}$), indicating that the adsorption rate in the initial stage is significantly faster. The negative value of $C_{(IP-1)}$ (-3.4163) suggests that the IP-1 line does not pass through the origin, indicating that intraparticle diffusion is not the sole rate-controlling mechanism and that film diffusion plays a significant role at the surface.

In the second stage (IP-2), the process is dominated by intraparticle diffusion into the internal pores of VCHA. The decrease in the k_{IP} value at this stage reflects a slower adsorption rate, as Pb(II) ions must penetrate narrower pore structures and approach the remaining active sites [6]. The positive value of $C_{(IP-2)}$ indicates increased diffusion resistance within the pores. At this stage, the amount of adsorbed Pb(II) increases more slowly and approaches a steady condition, leading the system toward equilibrium. The relatively low R^2 values for both stages indicate that intraparticle diffusion contributes only as one of the mechanisms involved, rather than being the primary rate-controlling mechanism in the Pb(II) adsorption system onto VCHA.

A further discussion on the adsorption rate constant of the Ho kinetic model (k_{Ho}), reveals that, although this model exhibits the highest R^2 value, it has certain limitations due to the limited number of parameters it provides. This makes it less suitable for cross-analysis with other models, including adsorption isotherm parameters. The Ho model only yields k_{Ho} and Calc. q_e values, whereas cross-analysis between kinetic and isotherm models requires additional information, such as the desorption rate constant (k_d) [15]. Therefore, the RBS kinetic model offers an advantage by enabling the determination of the desorption rate constant (k_d), allowing cross-analysis to be performed through the relationship $K = {k_a}/{k_d}$ with comparative parameters presented in Table 7.

The results indicate that the RBS model has a lower R^2 value than the Ho model but is relatively comparable to the Lagergren model. This suggests that the RBS kinetic model has optimal conditions similar to those of the Lagergren model. One of the determining variables is the initial concentration (C_o), with both the Lagergren and RBS models tending to yield higher R^2 values when C_o is in excess [6]. Based on Table 7, E_{RBS} (20.99 kJ/mol) is closest to E_L (23.95 kJ/mol). These results indicate that the RBS kinetic model is well-suited to describing Pb(II) adsorption onto VCHA and can be used to predict adsorption energy solely from kinetic data.

4. Conclusion

The extraction of humic acid from vermicompost (VCHA) was successfully achieved through an alkaline dissolution method using NaOH followed by acid precipitation with HCl, yielding a product with characteristic humic properties. UV–Vis analysis confirmed the presence of humic substances, as indicated by a strong absorption peak in the UV region at 280 nm followed by a gradual decrease at higher wavelengths, reflecting typical humic spectral behavior and a moderate degree of humification. In addition, VCHA exhibited a significantly higher total acidity compared to other humic acid sources such as HDHA, PSHA, and CDHA, indicating a greater abundance of active functional groups and enhanced potential as an alternative humic acid source. Adsorption studies demonstrated that VCHA possesses excellent performance in removing Pb(II) ions, with the process predominantly governed by chemisorption mechanisms. The adsorption equilibrium followed the Langmuir isotherm model, indicating monolayer adsorption on a homogeneous surface with a maximum adsorption capacity of 129.0463 mg/g. The relatively high adsorption energy (>20 kJ/mol), supported by Dubinin–Radushkevich analysis, suggests that ion-exchange interactions play a significant role in the adsorption process. Furthermore, kinetic modeling revealed that the adsorption follows a pseudo-second-order (Ho) model, confirming that chemical interactions between Pb(II) ions and negatively charged functional groups on the VCHA surface control the rate-limiting step. Overall, the high adsorption capacity, favorable adsorption

characteristics, and environmentally friendly nature of VCHA highlight its strong potential as a sustainable adsorbent for heavy metal wastewater treatment.

Acknowledgment

The authors sincerely acknowledge the financial support provided by the Department of Chemistry, Republic of Indonesia Defense University, and partially financed by LPDP and Badan Riset dan Inovasi Nasional (BRIN) (RIIM-4 contract: 152/IV/KS/11/2023 and PKS/206/XI/2023/UNHANRI). The authors also extend their gratitude for the facilities and laboratory resources made available by BRIN.

References

[1] C. S. T. Agustina, L. Lisdiana, Isolasi dan Karakterisasi Bakteri Pendegradasi Logam Timbal (Pb) di Perairan Teluk Lamong Surabaya, *LenteraBio: Berkala Ilmiah Biologi*, 12, 1, (2023), 101-106 https://doi.org/10.26740/lenterabio.v12n1.p101-106

[2] P. Zhao, A. Wang, P. Wang, Z. Huang, Z. Fu, Z. Huang, Two recyclable and complementary adsorbents of coal-based and bio-based humic acids: High efficient adsorption and immobilization remediation for Pb(II) contaminated water and soil, *Chemosphere*, 318, (2023), 137963 https://doi.org/10.1016/j.chemosphere.2023.137963

[3] S. Xue, Y. Hu, K. Wan, Z. Miao, Exploring Humic Acid as an Efficient and Selective Adsorbent for Lead Removal in Multi-Metal Coexistence Systems: A Review, *Separations*, 11, 3, (2024), 80 https://doi.org/10.3390/separations11030080

[4] J. W. Xu, Y. K. Wu, Y. Ding, T. W. Ji, W. Q. Zhu, Enhancing Pb^{2+} adsorption and microbial diversity in vermicompost with struvite, biochar, and shell powder, *Bioresource Technology Reports*, 32, (2025), 102345 https://doi.org/10.1016/j.biteb.2025.102345

[5] R. Basuki, S. J. Santosa, B. Rusdiarso, Ekstraksi Adsorben Ramah Lingkungan dari Matriks Biologi: Asam Humat Tinja Kuda (AH-TK), *Chempublish Journal*, 2, 1, (2017), 13-25

[6] R. Basuki, Y. B. Apriliyanto, E. Stiawan, A. R. Pradipta, B. Rusdiarso, B. R. Putra, Magnetic hybrid chitin-horse manure humic acid for optimized Cd(II) and Pb(II) adsorption from aquatic environment, *Case Studies in Chemical and Environmental Engineering*, 11, (2025), 101138 https://doi.org/10.1016/j.cscee.2025.101138

[7] P. B. Utomo, J. Nurdiana, Evaluasi Pembuatan Kompos Organik dengan Menggunakan Metode *Hot Composting*, *Jurnal Teknologi Lingkungan*, 2, 1, (2018), 28-32

[8] N. Nurlina, I. Syahbanu, M. T. Tamnasi, C. Nabela, Furnata, Ekstraksi dan Penentuan Gugus Fungsi Asam Humat dari Pupuk Kotoran Sapi, *Indonesian Journal of Pure and Applied Chemistry*, 1, 1, (2018), 30-38 https://doi.org/10.26418/indonesian.v1i1.26041

[9] M. S. A. Pohan, M. Purnamasari, F. Nisa, Ekstraksi dan Penentuan Gugus Fungsi Asam Humat dari Pupuk Kotoran Sapi Peternakan Yayasan Sasmita Jaya Serang, *Journal Crystal: Publikasi Penelitian Kimia dan Terapannya*, 7, 1, (2025), 40–45 https://doi.org/10.36526/jc.v7i1.4999

[10] T. Alomar, H. Qiblawey, F. Almomani, R. I. Al-Raoush, D. S. Han, N. M. Ahmad, Recent advances on humic acid removal from wastewater using adsorption process, *Journal of Water Process Engineering*, 53, (2023), 103679 https://doi.org/10.1016/j.jwpe.2023.103679

[11] J. Rani, S. Kumari, B. Paul, Extraction and chemical characterization of humic acid produced from lignite coals of arid region of Gujarat, Western India, *Scientific Reports*, 14, (2024), 30923 https://doi.org/10.1038/s41598-024-81861-6

[12] WenLi Cui, Ke Tang, Yunqiang Chen, Zhou Chen, Yihong Lan, YuBin Hong, WeiGuang Lan, Regulating the particle sizes of NaA molecular sieves toward enhanced heavy metal ion adsorption, *New Journal of Chemistry*, 48, 17, (2024), 7863-7874 https://doi.org/10.1039/D3NJ05924C

[13] K. Kustomo, Uji Karakterisasi dan Mapping Magnetit Nanopartikel Terlapisi Asam Humat dengan Scanning-Electron-Microscope-Energy Dispersive X-Ray (SEM-EDX), *Indonesian Journal of Chemical Science*, 9, 3, (2020), 148-153

[14] R. Basuki, B. Rusdiarso, S. J. Santosa, D. Siswanta, Magnetite-Functionalized Horse Dung Humic Acid (HDHA) for the Uptake of Toxic Lead(II) from Artificial Wastewater, *Adsorption Science & Technology*, 2021, (2021), 5523513 https://doi.org/10.1155/2021/5523513

[15] N. Ngatijo, N. Gusmaini, R. Bemis, R. Basuki, Adsorpsi Methylene Blue pada Nanopartikel Magnetit tersalut Asam Humat: Kajian Isoterm dan Kinetika, *CHEESA: Chemical Engineering Research Articles*, 4, 1, (2021), 51-64 https://doi.org/10.25273/cheesa.v4i1.8433.51-64

[16] D. C. Olk, P. R. Bloom, E. M. Perdue, D. M. McKnight, Y. Chen, A. Farenhorst, N. Senesi, Y.-P. Chin, P. Schmitt-Kopplin, N. Hertkorn, M. Harir, Environmental and Agricultural Relevance of Humic Fractions Extracted by Alkali from Soils and Natural Waters, *Journal of Environmental Quality*, 48, 2, (2019), 217-232 https://doi.org/10.2134/jeq2019.02.0041

[17] Adriana M. de Aquino, Luciano P. Canellas, Aminthia P. S. da Silva, Natália O. Canellas, Lívia da S. Lima, Fabio L. Olivares, Alessandro Piccolo, Riccardo Spaccini, Evaluation of molecular properties of humic acids from vermicompost by 13 C-CPMAS-NMR spectroscopy and thermochemolysis–GC–MS, *Journal of Analytical and Applied Pyrolysis*, 141, (2019), 104634 https://doi.org/10.1016/j.jaap.2019.104634

[18] J. Zhao, Y. Zhang, H. Cong, C. Zhang, J. Wu, Quantifying the contribution of lignin to humic acid structures during composting, *Chemical Engineering Journal*, 492, (2024), 152204 https://doi.org/10.1016/j.cej.2024.152204

[19] Zixin Zhang, Qi Chen, Guohua Ma, Kexin Zhang, Zhaoming Qu, Gaoyang E, Conghui Wang, Peng Zhang, Zhiguang Liu, Min Zhang, Jibiao Geng, Humic Acid Extracted from Danty via Catalytic Oxidation Using H_2O_2/Birnessite: Characteristics and Agricultural Beneficial Effects, *ACS Omega*, 7, 50, (2022), 47192-47201 https://doi.org/10.1021/acsomega.2c06411

[20] Yuling Liu, Haowei Zeng, Siduo Ding, Zhong Hu, Baiqing Tie, Si Luo, A new insight into the straw

decomposition associated with minerals: Promoting straw humification and Cd immobilization, *Journal of Environmental Sciences*, 148, (2025), 553-566 https://doi.org/10.1016/j.jes.2024.01.052

[21] Xuemei Yang, Jie Zhang, Khan M. G. Mostofa, Mohammad Mohinuzzaman, H. Henry Teng, Nicola Senesi, Giorgio S. Senesi, Jie Yuan, Yu Liu, Si-Liang Li, Xiaodong Li, Baoli Wang, Cong-Qiang Liu, Solubility characteristics of soil humic substances as a function of pH: mechanisms and biogeochemical perspectives, *Biogeosciences*, 22, 7, (2025), 1745-1765 https://doi.org/10.5194/bg-22-1745-2025

[22] Y. Ai, C. Zhao, L. Sun, X. Wang, L. Liang, Coagulation mechanisms of humic acid in metal ions solution under different pH conditions: A molecular dynamics simulation, *Science of The Total Environment*, 702, (2020), 135072 https://doi.org/10.1016/j.scitotenv.2019.135072

[23] Tu Lan, Peng Wu, Ziyi Liu, Martin Stroet, Jiali Liao, Zhifang Chai, Alan E. Mark, Ning Liu, Dongqi Wang, Understanding the Effect of pH on the Solubility and Aggregation Extent of Humic Acid in Solution by Combining Simulation and the Experiment, *Environmental Science & Technology*, 56, 2, (2022), 917-927 https://doi.org/10.1021/acs.est.1c05938

[24] Mona A. Darweesh, Mahmoud Y. Elgendy, Mohamed I. Ayad, AbdelMonem M. Ahmed, N. M. Kamel Elsayed, W. A. Hammad, Adsorption isotherm, kinetic, and optimization studies for copper (II) removal from aqueous solutions by banana leaves and derived activated carbon, *South African Journal of Chemical Engineering*, 40, (2022), 10-20 https://doi.org/10.1016/j.sajce.2022.01.002

[25] M. K. Sari, R. Basuki, B. Rusdiarso, Adsorption of Pb(II) from Aqueous Solutions onto Humic Acid Modified by Urea-Formaldehyde: Effect of pH, Ionic Strength, Contact Time, and Initial Concentration, *Indonesian Journal of Chemistry*, 21, 6, (2021), 1371-1388 https://doi.org/10.22146/ijc.64600

[26] Q. Xu, Y. Yan, Y. Jiao, J. Wu, X. Yan, X. Su, Highly Efficient Adsorption of Pb(II) by Functionalized Humic Acid: Molecular Experiment and Theoretical Calculation, *Materials*, 16, 23, (2023), 7290 https://doi.org/10.3390/ma16237290

[27] I. Usman, Y. A. Mohamad, E. Isa, Kandungan Timbal, Besi, dan Kadmium Pada Air dan Ikan Nike di Perairan Sungai Bone, Kota Gorontalo Menggunakan Metode Spektroskopi, *Journal of Health Sciences: Gorontalo Journal of Health Sciences and Community*, 9, 2, (2025), 150-164 https://doi.org/10.35971/gojhes.v9i2.29088

[28] M. R. Septiawan, I. Asnawi, F. R. Rahman, A. Ramadhan, Studi Khelasi Logam Timbal (Pb) Menggunakan Asam Sitrat, *Jurnal Teknologi Kimia dan Mineral*, 2, 1, (2023), 11-16 https://doi.org/10.61844/jtkm.v2i1.382

[29] J. Serafin, B. Dziejarski, Application of isotherms models and error functions in activated carbon CO_2 sorption processes, *Microporous and Mesoporous Materials*, 354, (2023), 112513 https://doi.org/10.1016/j.micromeso.2023.112513

[30] Rongping Chen, Yinlong Zhang, Lianfeng Shen, Xiaoyan Wang, Jianqiang Chen, Aijun Ma, Weimin Jiang, Lead(II) and methylene blue removal using a fully biodegradable hydrogel based on starch immobilized humic acid, *Chemical Engineering Journal*, 268, (2015), 348-355 https://doi.org/10.1016/j.cej.2015.01.081

[31] P. Bartczak, M. Norman, L. Klapiszewski, N. Karwańska, M. Kawalec, M. Baczyńska, M. Wysokowski, J. Zdarta, F. Ciesielczyk, T. Jesionowski, Removal of nickel(II) and lead(II) ions from aqueous solution using peat as a low-cost adsorbent: A kinetic and equilibrium study, *Arabian Journal of Chemistry*, 11, 8, (2018), 1209-1222 https://doi.org/10.1016/j.arabjc.2015.07.018

[32] A. Kushwaha, R. Rani, J. K. Patra, Adsorption kinetics and molecular interactions of lead [Pb(II)] with natural clay and humic acid, *International Journal of Environmental Science and Technology*, 17, 3, (2020), 1325-1336 https://doi.org/10.1007/s13762-019-02411-6

[33] T. Zehra, L. B. L. Lim, N. Priyantha, Characterization of peat samples collected from Brunei Darussalam and their evaluation as potential adsorbents for Cu(II) removal from aqueous solution, *Desalination and Water Treatment*, 57, 44, (2016), 20889-20903 https://doi.org/10.1080/19443994.2015.1110838

[34] M. Musah, Y. Azeh, J. Mathew, M. T. Umar, Z. Abdulhamid, A. I. Muhammad, Adsorption Kinetics and Isotherm Models: A Review, *Caliphate Journal of Science and Technology*, 4, 1, (2022), 20-26 https://doi.org/10.4314/cajost.v4i1.3

[35] N. Zhang, F. Reguyal, S. Praneeth, A. K. Sarmah, A novel green synthesized magnetic biochar from white tea residue for the removal of Pb(II) and Cd(II) from aqueous solution: Regeneration and sorption mechanism, *Environmental Pollution*, 330, (2023), 121806 https://doi.org/10.1016/j.envpol.2023.121806